Supplementary Information

Collaborative multi-interface engineering and dynamic iron exchange boost robust bifunctional water electrolysis at 2 A cm^{-2}

1. Experimental section

Synthesis of the $NiMoO_4$ precursor. $NiMoO_4$ precursor was synthesized on Ni foam by a hydrothermal method. 0.04 M $Ni(NO_3)_2 \cdot 6H_2O$ and 0.01M $(NH_4)_6Mo_7O_{24} \cdot 4H_2O$ were dissolved into 40 mL ultrapure water and stirred for 15 min at room temperature, which was then transferred into a 100 mL Teflon-lined autoclave with a piece of nickel foam. After a hydrothermal process at 150 °C for 6 h in drying oven, the as-prepared $NiMoO_4$ samples were cleaned by ultrapure water and dried in room temperature.

Synthesis of the $Fe/MoNi_4/MoO_2$ nanoarray. $NiMoO_4$ precursor was soaked in ferric nitrate ink for a few seconds. After drying at room temperature overnight, the as-prepared samples were placed at the center of the tube furnace, which was then heated to 400 °C with a duration of 2 h under H_2/Ar atmosphere to obtain the final $Fe/MoNi_4/MoO_2$. After that, the as-prepared samples were cooled down to room temperature and passivated overnight under Ar atmosphere.

Synthesis of the $MoNi_4/MoO_2$ and Ar-$NiMoO_4$ samples. $NiMoO_4$ precursor was directly treated in Ar or H_2/Ar (8:92) atmosphere using the same conditions to obtain Ar-$NiMoO_4$ and $MoNi_4/MoO_2$ samples, respectively.

Synthesis of $FeMo/MoO_2$. $FeMo/MoO_2$ was prepared following the same procedure for

$MoNi_4/MoO_2$ by changing $Ni(NO_3)_2 \cdot 6H_2O$ into $Fe(NO_3)_3 \cdot 9H_2O$ during the hydrothermal treatment.

Synthesis of MoO_2. MoO_2 was prepared following the same procedure for $MoNi_4/MoO_2$ with the absence of $Ni(NO_3)_2 \cdot 6H_2O$.

Electrochemical measurements. All the electrochemical measurements were performed in 100 mL 1 M KOH (pH = 14) or 100 mL 1M PBS (pH ≈ 6.5) solutions at room temperature based on the standard three-electrode system. In 1 M KOH, the as-prepared samples were used as working electrode, Hg/HgO electrode and graphite rod were assigned as reference and counter electrodes, respectively. The linear polarization curves were obtained at a scan rate of 2 mV s^{-1} by linear sweep voltammetry mode. Before testing, all the catalysts were electrochemically activated by 50 cyclic voltammetry at a scan rate of 50 mV s^{-1} with the potentials from 0.05 V to -0.23 V (HER) and 1.124 V to 1.574 V (OER). The EIS spectra were tested at -0.05 V for HER and 1.53 V for OER along with the frequencies varying from 0.1 Hz to 100 kHz. In 1 M PBS, graphite rod and saturated calomel electrode were employed as the counter and reference electrodes, respectively. During all the data measurements, on-the-fly *iR* compensation was automatically performed for all the polarization curves by the workstation system (Gamry Reference 3000 or 600+).[1]

Electrochemical active surface area (ECSA) calculation. The ECSA can be estimated on the basis of the follow equation: ECSA = $\frac{C\mathrm{dl}}{C\mathrm{s}}$, where C_s is the capacitance per unit area of an electrode with very flat surface, and C_{dl} is related to the double-layer capacitances of our porous electrodes measured by an electrochemical method.[2,3] Here the value of C_s = 40 μF cm^{-2} was selected for ECSA calculation.

Turnover frequency (TOF) calculation. TOF was calculated according to the following equation: $\mathrm{TOF} = \frac{j}{\mathrm{N} \times \mathrm{n_s} \times F}$, where j is the HER current density, N is the number of electrons transferred per H_2 molecule (N = 2), F represents the Faraday constant, and n_s represents the density of total active sites per unit area of electrode material. The number of active sites for HER was evaluated according to this formula: $\mathrm{n_s} = \frac{Q}{2\mathrm{F}S}$, where S, F and Q correspond to the geometric area of the electrode materials, Faraday constant and the whole charge of cyclic voltammetry curve collected in 1M PBS electrolyte (pH ≈ 6.5).

In-situ **Raman measurements.** The Raman spectra were recorded under a 532 nm laser (Horiba JY HR Evolution). A typical three-electrode configuration (Beijing Scistar Technology Co. Ltd) was designed for in-situ Raman measurements, in which the self-supported catalyst, AgCl/Ag and Pt wire were served as the working, reference and counter electrodes, respectively. The potential was controlled by an electrochemical workstation, as described previously, with applied potentials ranging from 1.12 to 1.72 V. Before collecting the Raman spectra at each potential, chronoamperometric tests were conducted on the OER catalysts for five minutes.

In-situ **XPS measurements.** The X-ray photoelectron (XPS) spectra were tested by a XPS spectroscopy (Thermo Fisher Scientific-Escalab 250Xi) with an analyzer pass energy of 30 eV and a dwell time of 50 ms. The chamber pressure was remained below 4.3×10^{-7} during the tests. For the in-situ XPS tests, a self-assembly three-electrode setup (working, reference and counter electrodes) was employed for OER testing, in which the OER catalyst, Hg/HgO electrode and Pt wire were served as working, reference and counter electrodes, respectively. The samples were tested at different anodic potentials ranging from 1.12 to 1.72 V for 30 min

in a glovebox continuously purged by N_2 gas (Suzhou Vigor Technologies Co., Ltd.). Following the OER tests, the samples were dried and transferred to the XPS spectrometer under N_2 atmosphere.

Fine structure characterization. Fe K-edge X-ray absorption spectra (XAS) were recorded in a transmission mode at the 1W1B and 1W2B beamlines of the Beijing Synchrotron Radiation Facility in China.

Computational method. Spin-polarized density functional theory (DFT) calculations were performed with the Vienna Ab Initio Simulation Package (VASP 5.3.5).[4] In our calculations, we adopted the Perdew-Burke-Ernzerhof (PBE) functional to consider exchange and correlation effects.[5] A cutoff energy of 400 eV was used for the plane-wave basis. The Gaussian smearing method with a smearing width of 0.03 eV was used to determine partial occupancies. DFT-D3 method was used to take into account the VdW interactions.[6]

Our calculated lattice constants of bulk $MoNi_4$ are a= 5.64 Å and c = 3.53 Å. For bulk MoO_2, the optimized lattice constants are a = 4.92 Å and c = 2.75 Å. The calculated bulk structures were used to construct surface models. A 2 × 2 unit cell of $MoNi_4$ (200) with eight atomic layers was considered in our calculations. Here, the top four atomic layers were relaxed, and the bottom four layers were frozen. For comparison, the MoO_2 (110) surface was constructed with also six atomic layers. Here, we optimized the top three atomic layers and fixed the bottom three layers. In this work, the interfaces of Fe/$MoNi_4$ (200) and Fe/MoO_2 (110) models were modelled by Fe_4 cluster placed on $MoNi_4$ (200) and MoO_2 (110) surfaces. The size of $MoNi_4$ (200) and Fe/$MoNi_4$ (200) unit cells both were 11.37 Å × 10.78 Å × 20.11 Å. For the MoO_2 (110) and Fe/MoO_2 (110), we used the unit cell of 11.00 Å × 13.90 Å ×

20.46 Å. The atom-layer slab separated by a 15 Å vacuum was considered for all the calculations. All the supercells in our DFT calculations are large enough to avoid interactions between periodic images that would affect the results of the predicted surface catalytic properties involving the small adsorbates. For the Brillouin zone integration, a Monkhorst-Pack k-point mesh of 3× 3× 1 was used. Structure optimization was finished until the residual Hellmann-Feynman forces were smaller than 0.02 eV/Å.

To explore the energy barriers for water dissociation on the catalysts, we calculated the location and total electronic energy of transition states by the climbing-image nudged elastic band (CI-NEB) method.[7] A frequency analysis was performed to confirm that each transition state has a single imaginary frequency in the direction of the reaction coordinate. The Gibbs free energies of hydrogen and water at 298.15 K and 1 atm were calculated with

$$G = E_{DFT} + E_{ZPE} - TS \qquad (1)$$

Where G is Gibbs free energy, E_{DFT} is the electronic total energy from DFT calculation, E_{ZPE} is the zero-point energy of the calculated system, T stands for the Kelvin temperature and S represents the entropy. Free energy of hydrogen and water adsorption were calculated by

$$\Delta G_{ads} = G_{surf+M} - (G_{surf} + G_{M}) \qquad (2)$$

Here, $G_{\mathrm{surf+M}}$ and G_{surf} are the free energies of atomic hydrogen atom or water adsorbed surface, and the catalytic surface, respectively. For the free energy of atomic hydrogen adsorption, G_{M} is half of the free energies of the gas phase hydrogen. For the free energy of molecular water adsorption, G_{M} is the free energy of the gas phase water molecule.

2. Material characterization and electrochemical analysis

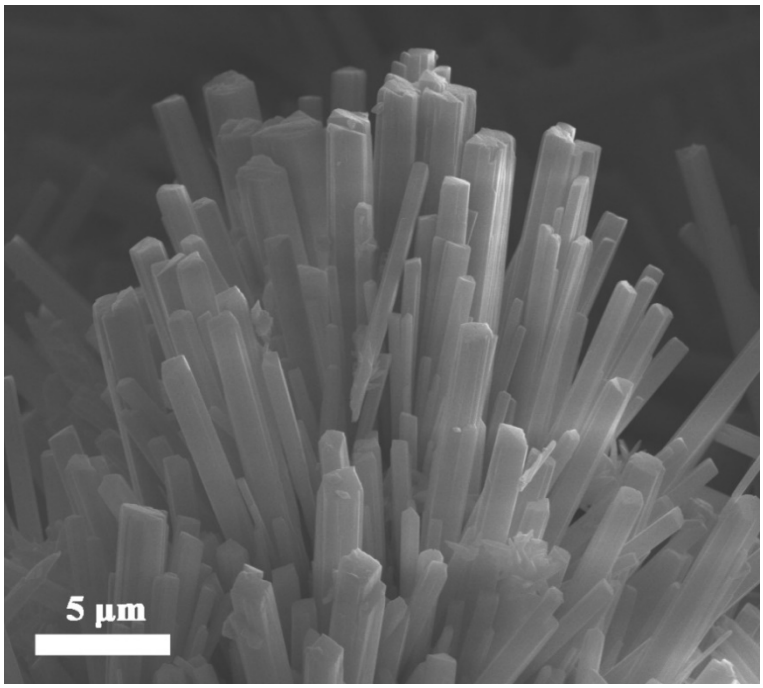

Supplementary Fig. 1. SEM image of $NiMoO_4$ precursor.

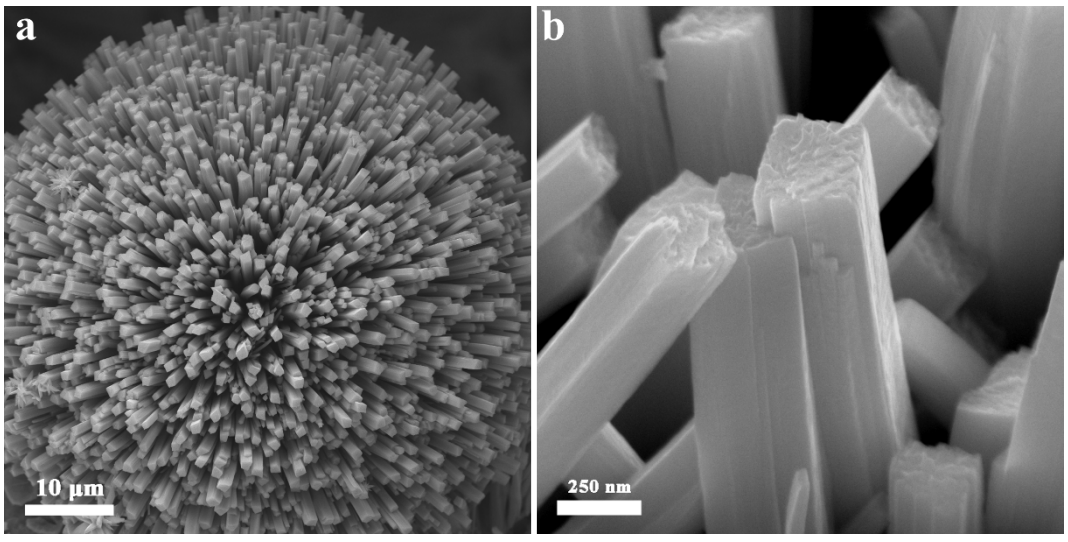

Supplementary Fig. 2. SEM images of $MoNi_4/MoO_2$ nanoarray.

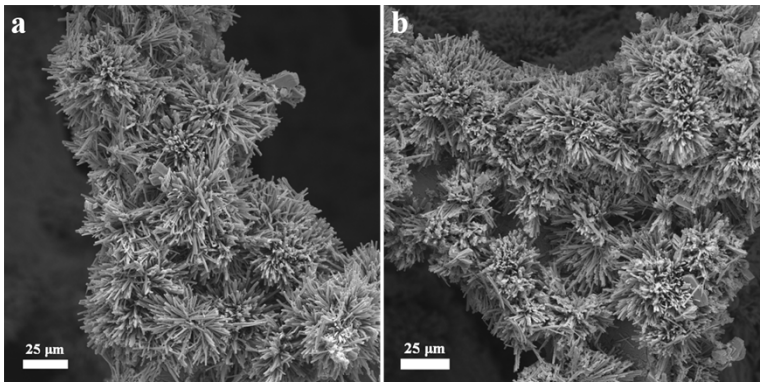

Supplementary Fig. 3. SEM images of the as-prepared Fe/$MoNi_4$/MoO_2 nanoarray.

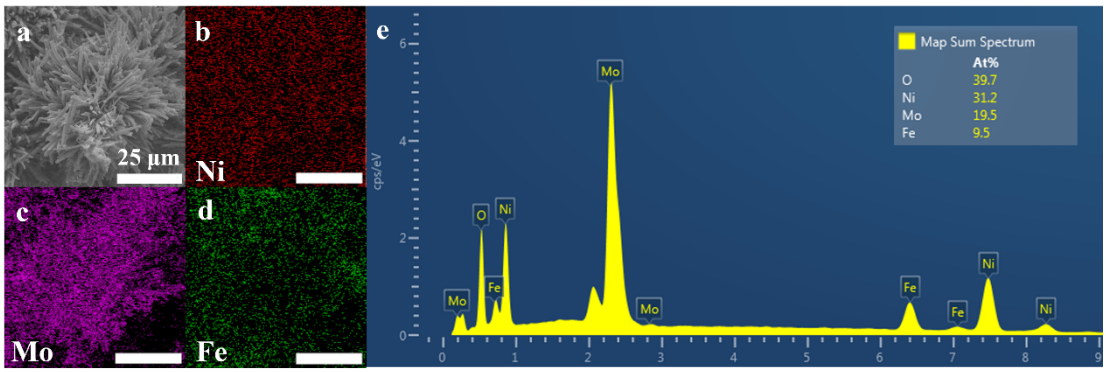

Supplementary Fig. 4. (a) SEM image of Fe/$MoNi_4$/MoO_2 nanorod and corresponding elemental mapping images of (b) Ni, (c) Mo and (d) Fe. (e) A typical EDX spectrum of Fe/$MoNi_4$/MoO_2 nanoarray.

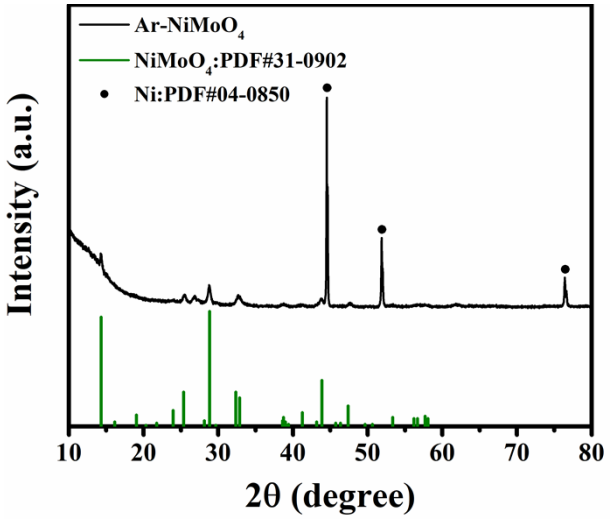

Supplementary Fig. 5. A typical XRD pattern of the Ar-$NiMoO_4$ nanorods on Ni foam.

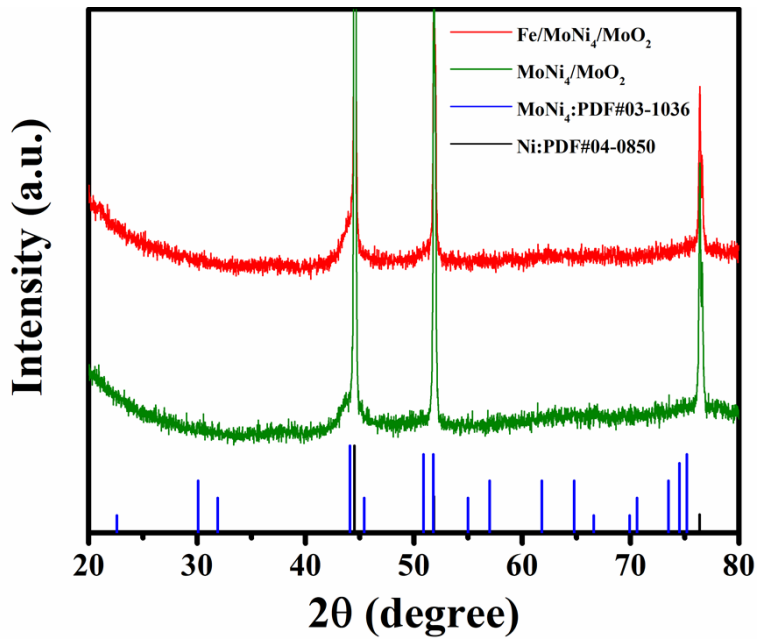

Supplementary Fig. 6. XRD spectra of $Fe/MoNi_4/MoO_2$ (red line) and $MoNi_4/MoO_2$ (green line) nanoarray grown on Ni foam.

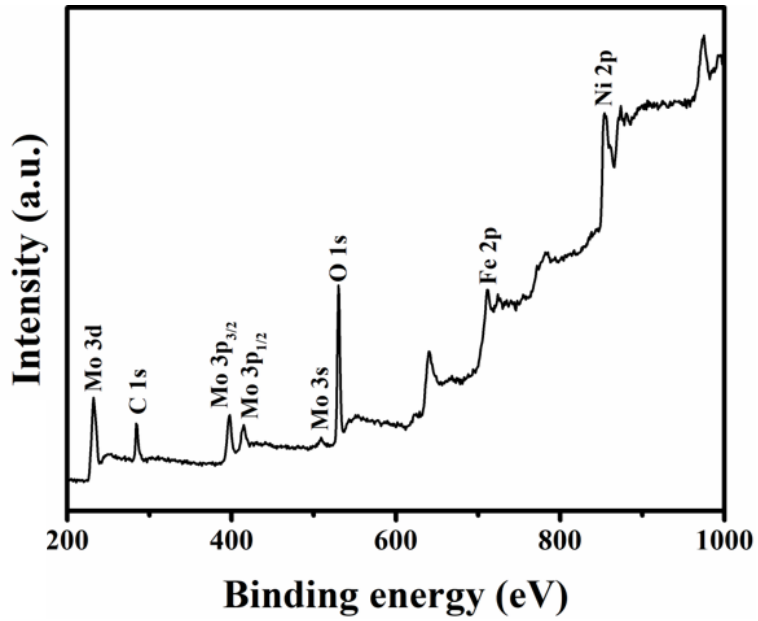

Supplementary Fig. 7. The XPS survey spectra of $Fe/MoNi_4/MoO_2$ nanoarray.

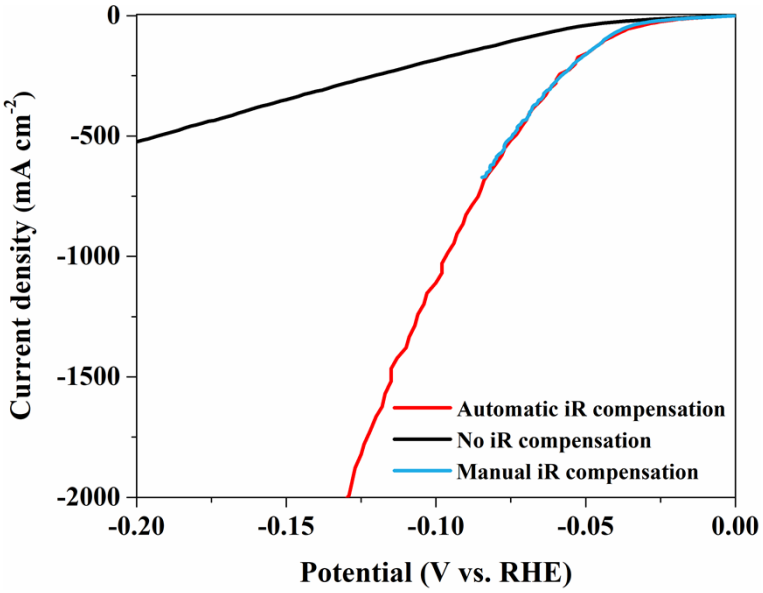

Supplementary Fig. 8. The HER polarization curves of $Fe/MoNi_4/MoO_2$ with automatic, manual (100%) *iR* compensation or without compensation.

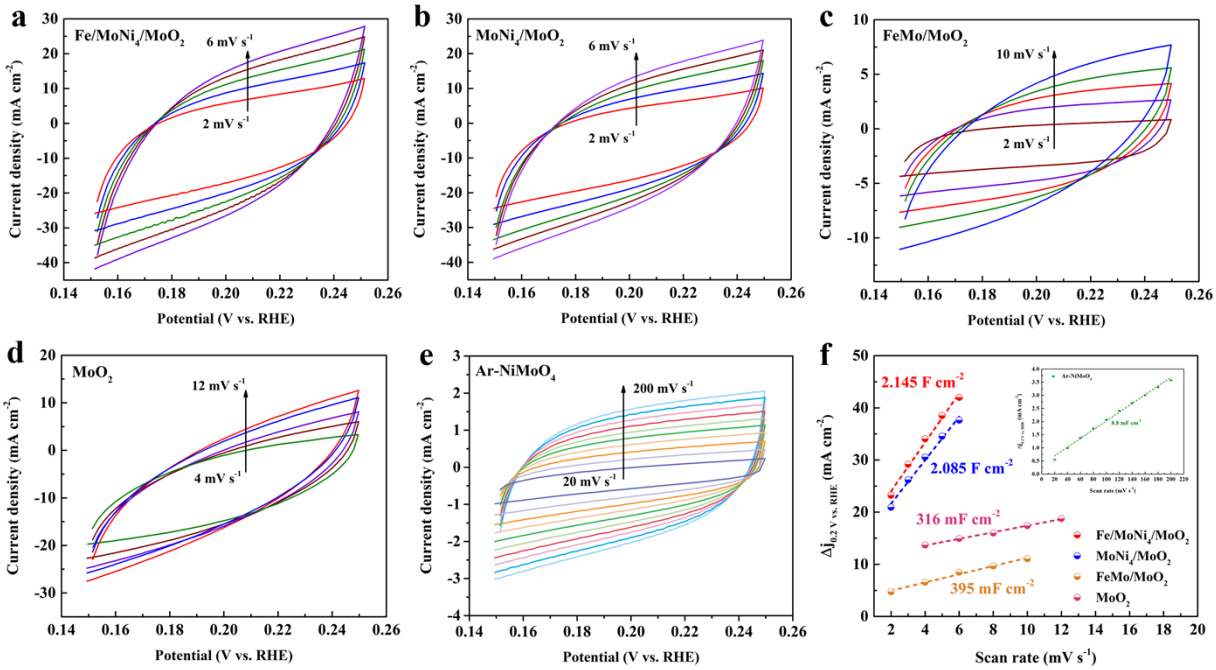

Supplementary Fig. 9. Typical cyclic voltammetry curves collected on (a) $Fe/MoNi_4/MoO_2$, (b) $MoNi_4/MoO_2$, (c) $FeMo/MoO_2$, (d) MoO_2 and (e) $Ar\text{-}NiMoO_4$ electrodes in 1 M KOH with different scan rates. (f) The double-layer capacitance (C_{dl}) of $Fe/MoNi_4/MoO_2$, $MoNi_4/MoO_2$, $FeMo/MoO_2$, MoO_2 and $Ar\text{-}NiMoO_4$ electrodes in 1 M KOH.

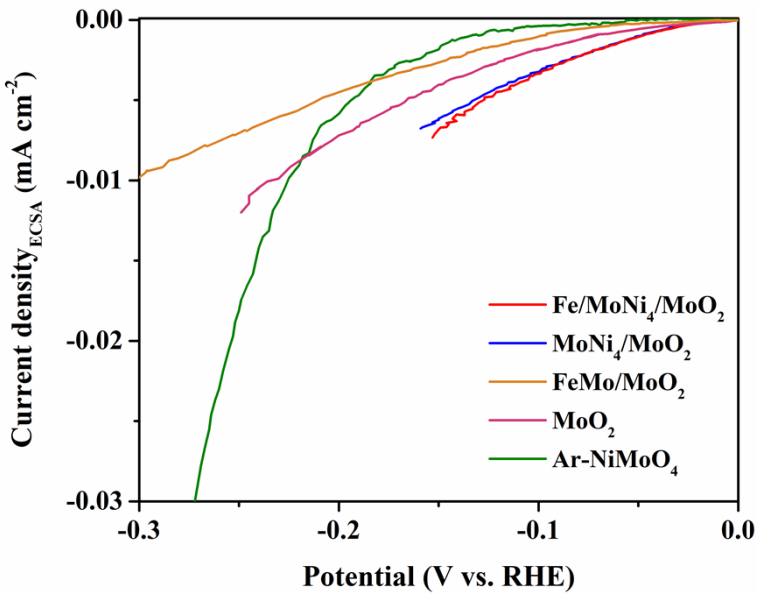

Supplementary Fig. 10. The ECSA-normalized HER polarization curves of $Fe/MoNi_4/MoO_2$, $MoNi_4/MoO_2$, $FeMo/MoO_2$, MoO_2 and $Ar\text{-}NiMoO_4$ electrodes.

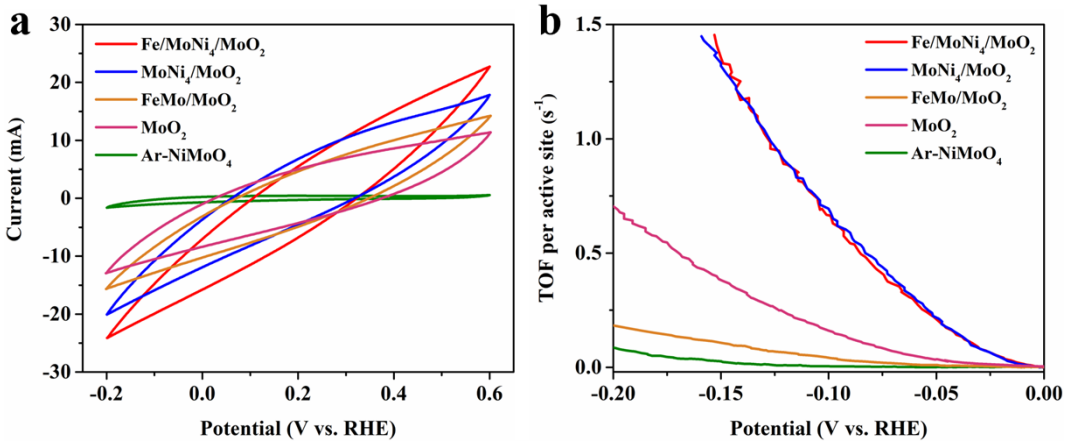

Supplementary Fig. 11. (a) The cyclic voltammetry curves collected on $Fe/MoNi_4/MoO_2$, $MoNi_4/MoO_2$, $FeMo/MoO_2$, MoO_2 and $Ar\text{-}NiMoO_4$ electrodes at a scan rate of 50 mV s^{-1} in 1 M PBS. (b) The corresponding TOF values of these catalysts for the HER in 1 M KOH.

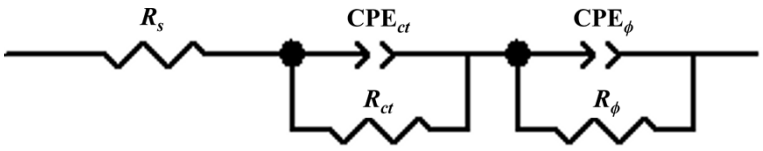

Supplementary Fig. 12. The schematic diagram of equivalent circuit. R_s: series resistance,

CPE_{ct}: charge transfer constant phase element, R_{ct}: charge transfer resistance, CPE_{ϕ}: ionic intermediate adsorption constant phase element, R_{ϕ}: ionic intermediate adsorption resistance.

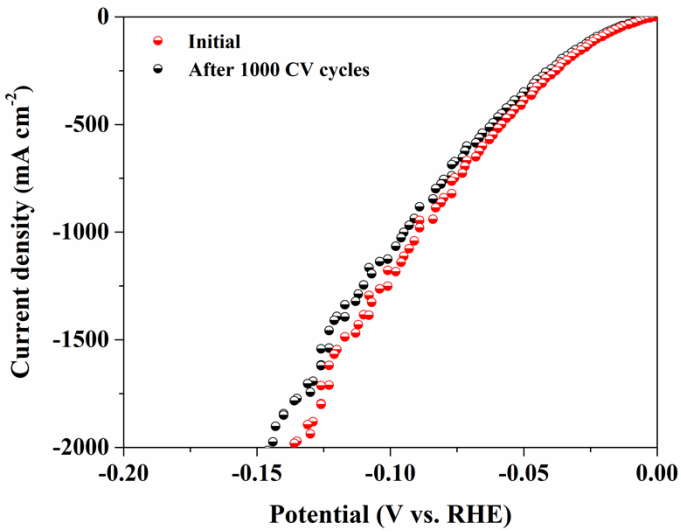

Supplementary Fig. 13. Cyclic stability of $Fe/MoNi_4/MoO_2$ nanoarray for HER.

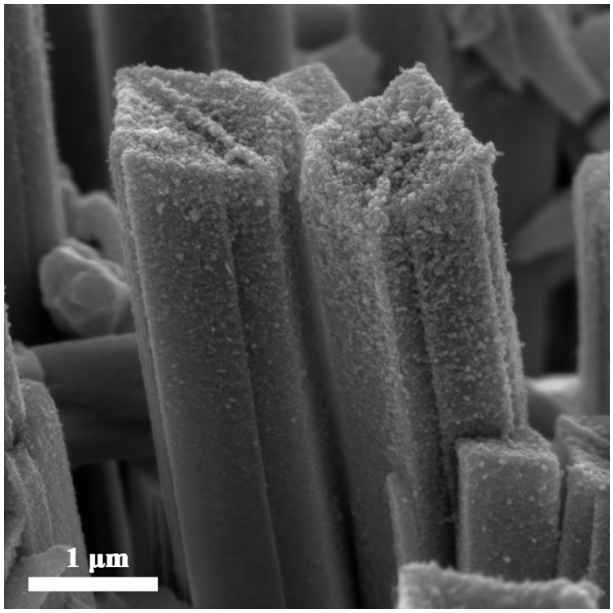

Supplementary Fig. 14. The SEM image of post-HER $Fe/MoNi_4/MoO_2$ nanoarray.

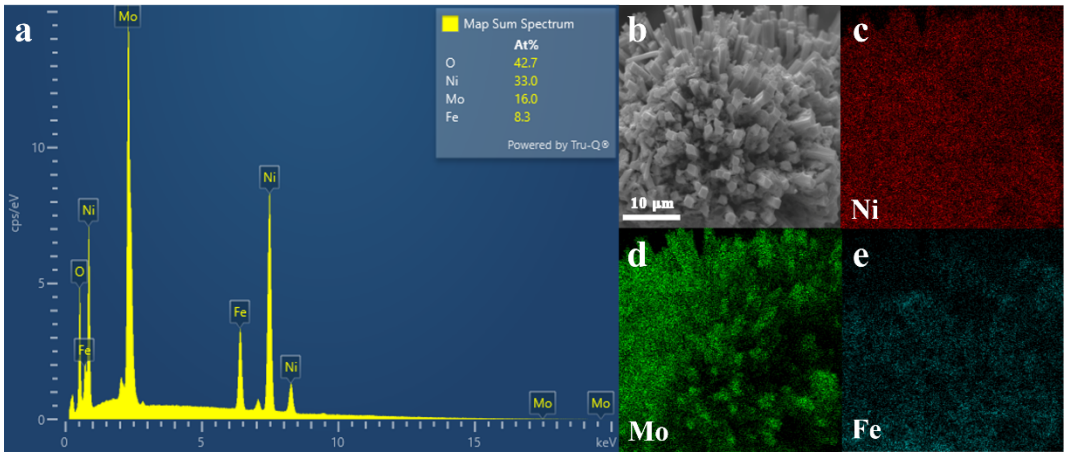

Supplementary Fig. 15. (a) A typical EDX spectrum for Fe/$MoNi_4$/MoO_2 sample after HER and the atomic ratios of O, Ni, Mo and Fe elements were shown in the inset. (b) SEM image of Fe/$MoNi_4$/MoO_2 after HER cycling test and corresponding EDS mapping of (c) Ni, (d) Mo and (e) Fe elements.

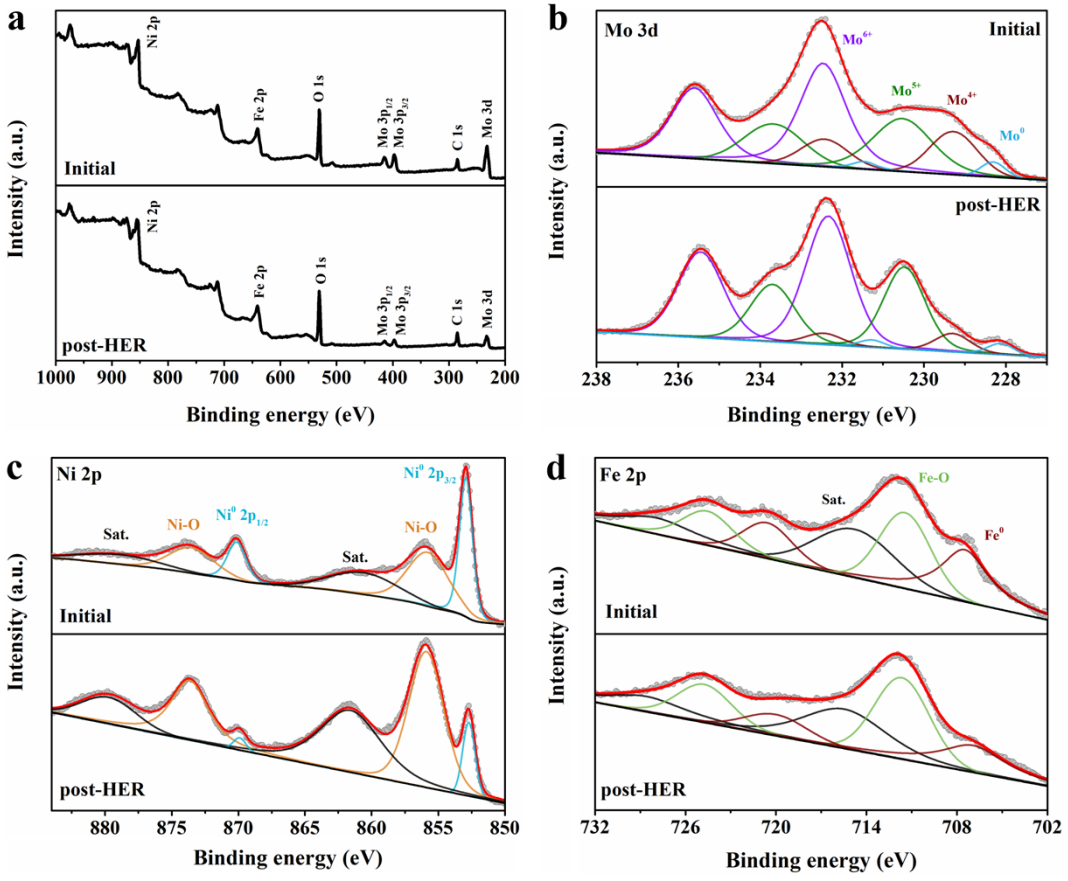

Supplementary Fig. 16. (a) The XPS survey and corresponding high-resolution spectra of (b)

Mo 3d, (e) Ni 2p, (d) Fe 2p for original (top) and post-HER Fe/$MoNi_4$/MoO_2 (bottom).

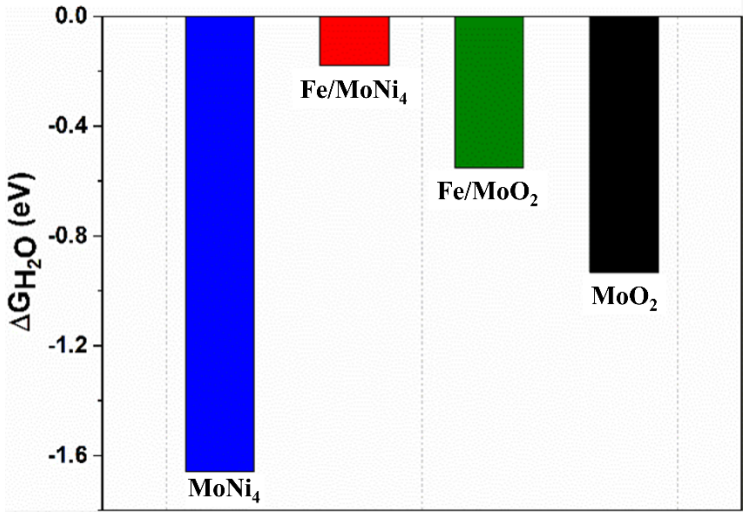

Supplementary Fig. 17. Adsorption free energy of water on $MoNi_4$, Fe/$MoNi_4$, Fe/MoO_2 and MoO_2 catalysts.

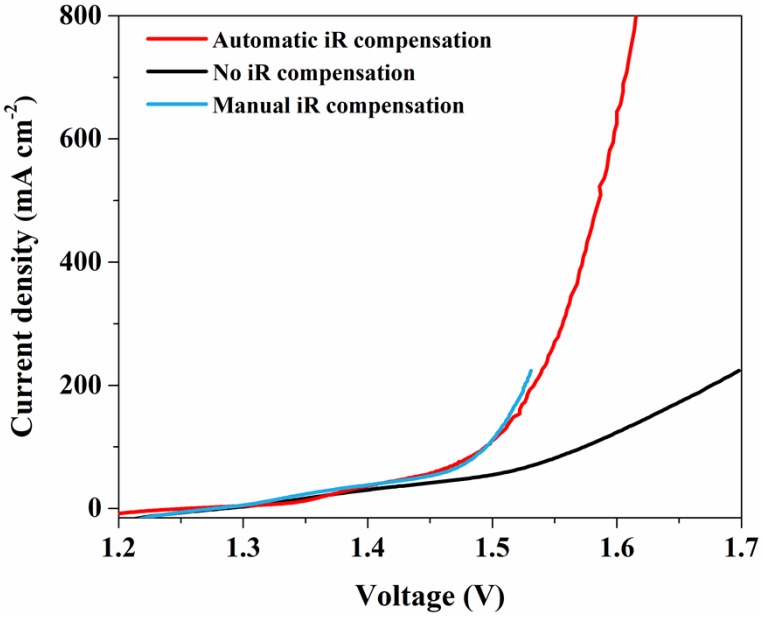

Supplementary Fig. 18. The polarization curves of Fe/$MoNi_4$/MoO_2 for OER with automatic, manual (100%) *iR* compensation or without compensation.

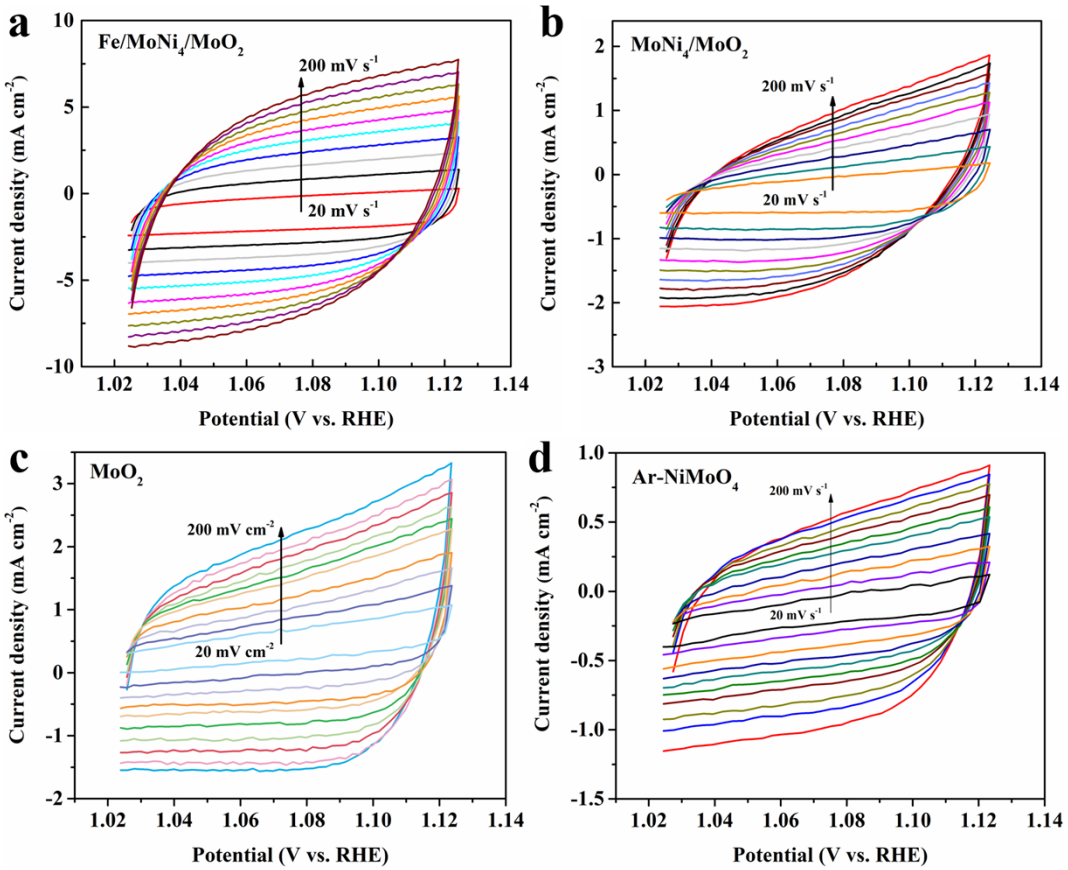

Supplementary Fig. 19. Cyclic voltammetry curves of (a) $Fe/MoNi_4/MoO_2$, (b) $MoNi_4/MoO_2$, (c) MoO_2 and (d) $Ar\text{-}NiMoO_4$ catalysts at various scan rates from 20 to 200 mV s^{-1}.

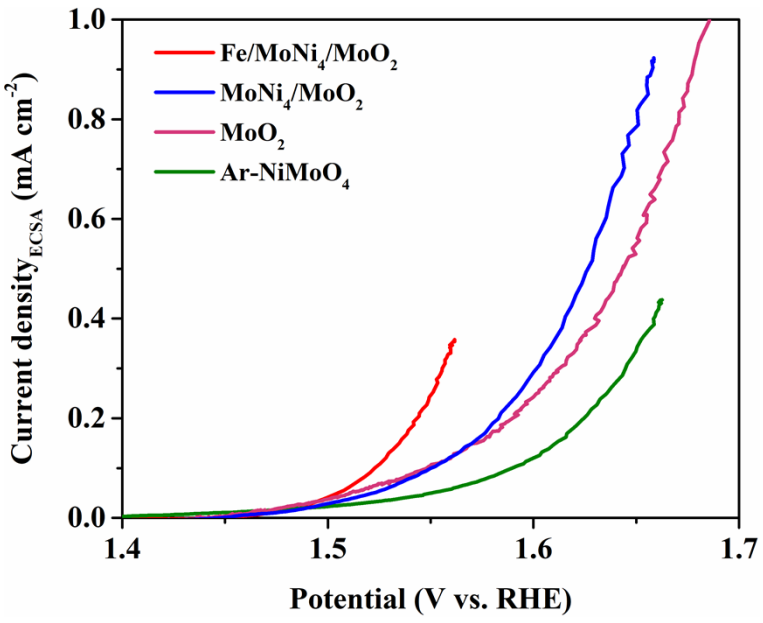

Supplementary Fig. 20. The ECSA-normalized OER polarization curves of $Fe/MoNi_4/MoO_2$, $MoNi_4/MoO_2$, MoO_2 and $Ar\text{-}NiMoO_4$ electrodes.

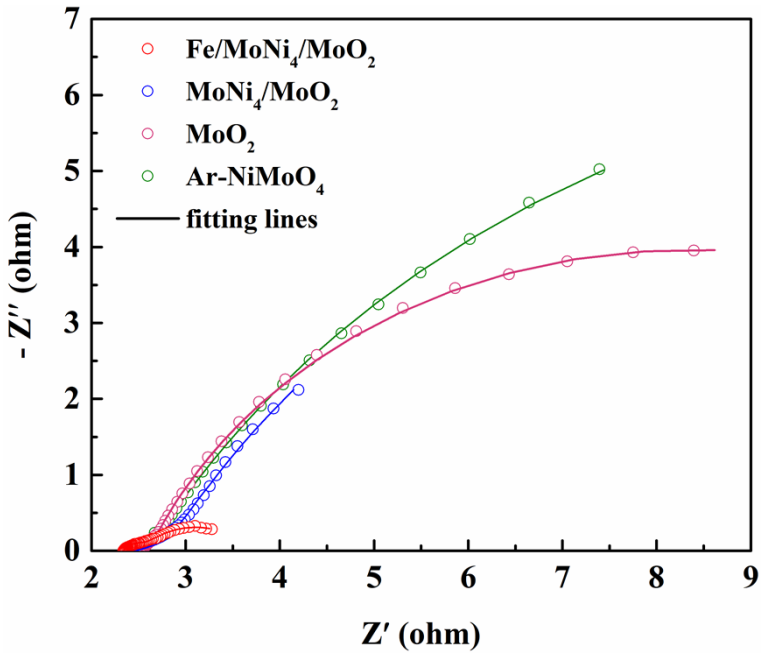

Supplementary Fig. 21. The Nyquist plots of $Fe/MoNi_4/MoO_2$, $MoNi_4/MoO_2$, MoO_2 and Ar-$NiMoO_4$ catalysts in 1 M KOH at 1.53 V.

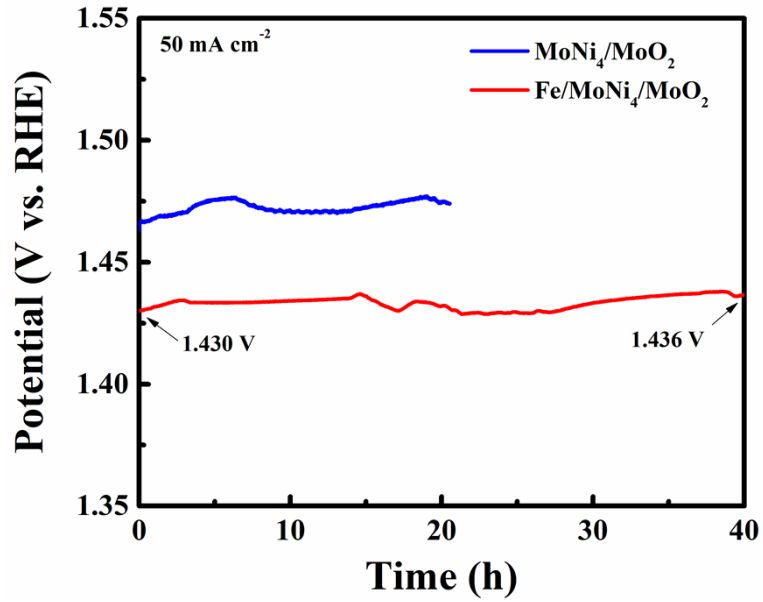

Supplementary Fig. 22. Long-term stability tests of $Fe/MoNi_4/MoO_2$ and $MoNi_4/MoO_2$ catalysts for OER at current density of 50 mA cm^{-2} in 1 M KOH.

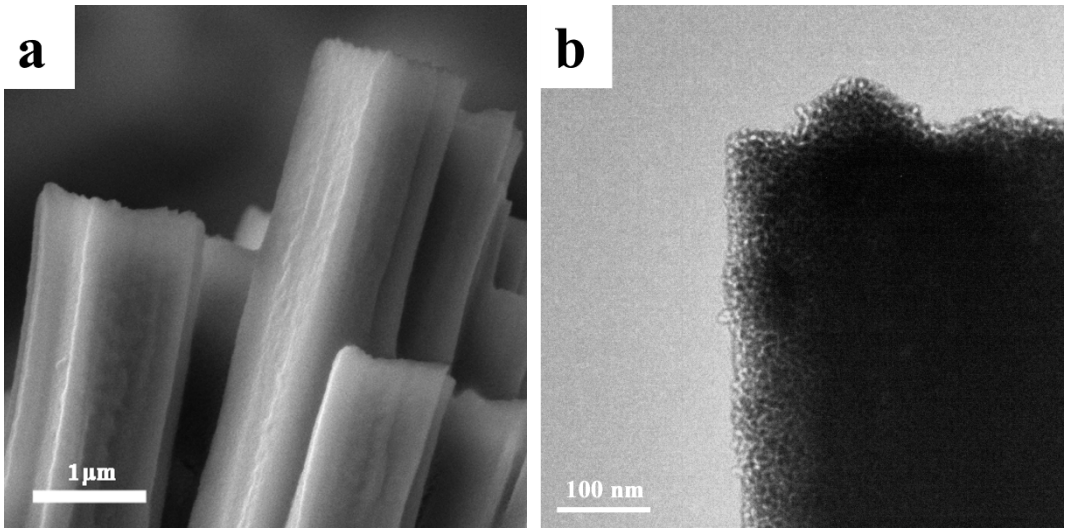

Supplementary Fig. 23. (a) SEM image and (b) TEM image of post-OER Fe/$MoNi_4$/MoO_2.

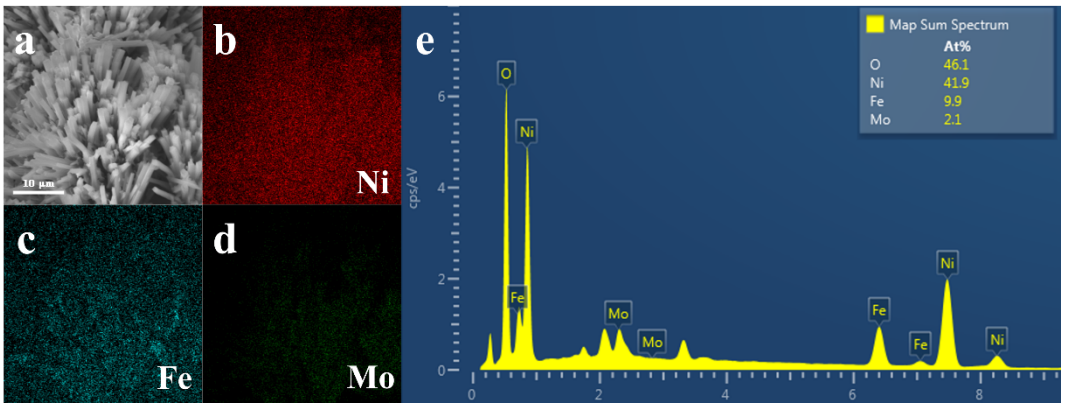

Supplementary Fig. 24. (A) SEM image of post-OER Fe/$MoNi_4$/MoO_2 and corresponding EDS mapping of (b) Ni, (c) Fe and (d) Mo elements. (e) A typical EDX spectrum for Fe/$MoNi_4$/MoO_2 sample after OER and the atomic ratios of O, Ni, Mo and Fe elements were shown in the inset.

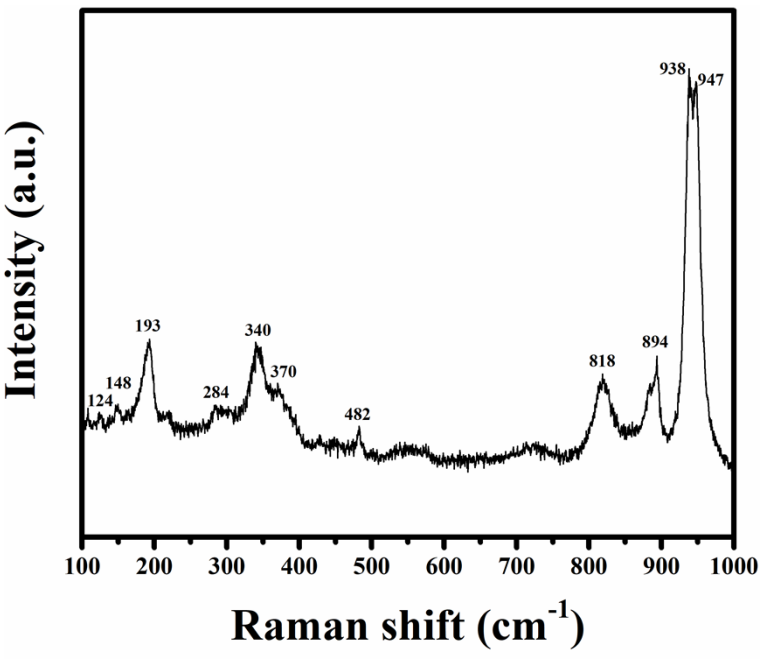

Supplementary Fig. 25. Raman spectra of initial Fe/$MoNi_4$/MoO_2 sample.

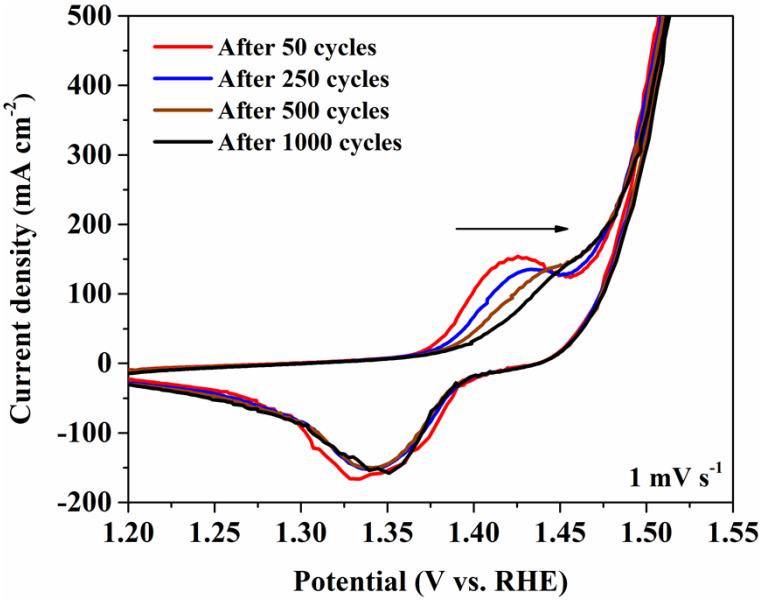

Supplementary Fig. 26. The linear polarization curves of Fe/$MoNi_4$/MoO_2 collected after different CV cycles.

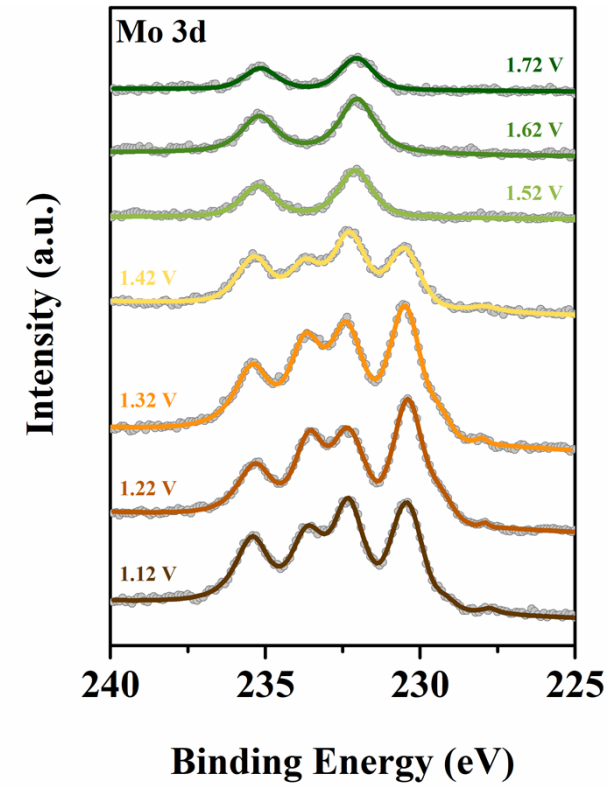

Supplementary Fig. 27. *In-situ* XPS spectra of Mo 3d for Fe/$MoNi_4$/MoO_2 during OER.

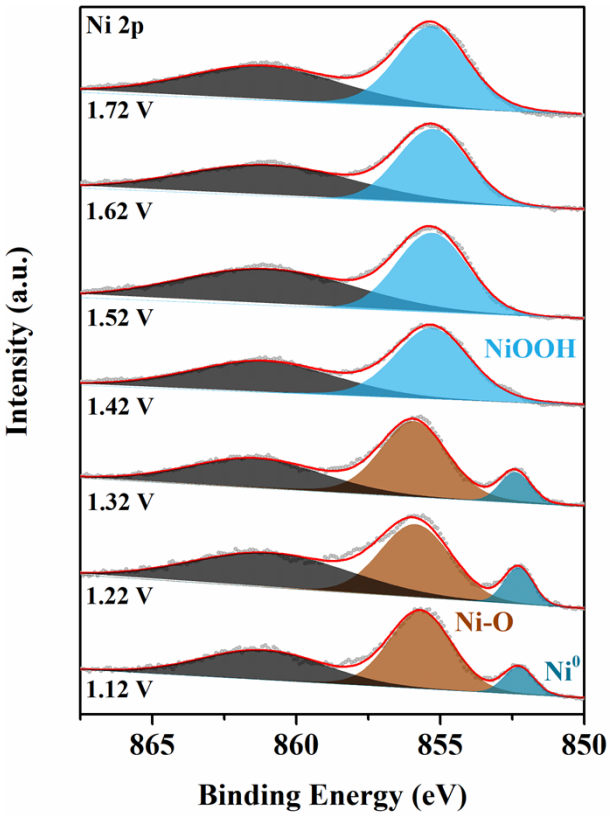

Supplementary Fig. 28. *In-situ* XPS spectra of Ni 2p for $MoNi_4$/MoO_2 during OER.

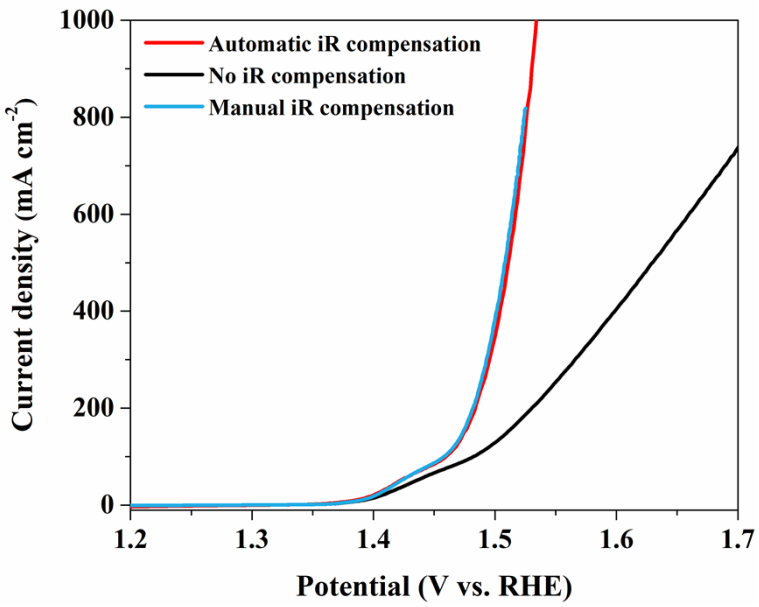

Supplementary Fig. 29. The overall-water-splitting polarization curves of Fe/$MoNi_4$/MoO_2|| Fe/$MoNi_4$/MoO_2 with automatic, manual (100%) *iR* compensation or without compensation.

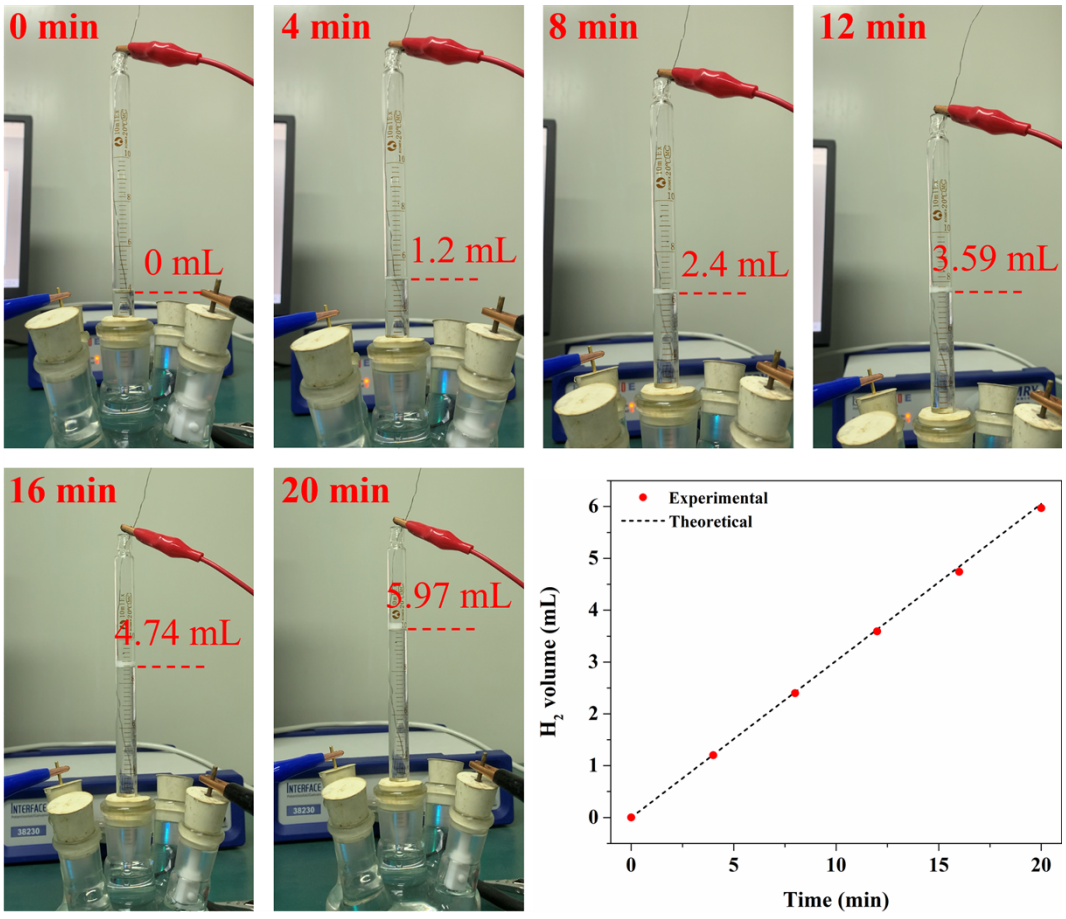

Supplementary Fig. 30. Measuring H_2 gas volume and determining the Faradaic efficiency

by comparing experimental (red dot) and theoretical (black line) H_2 amounts using a drainage method during HER catalysis at 200 mA cm^{-2} in 1M KOH.

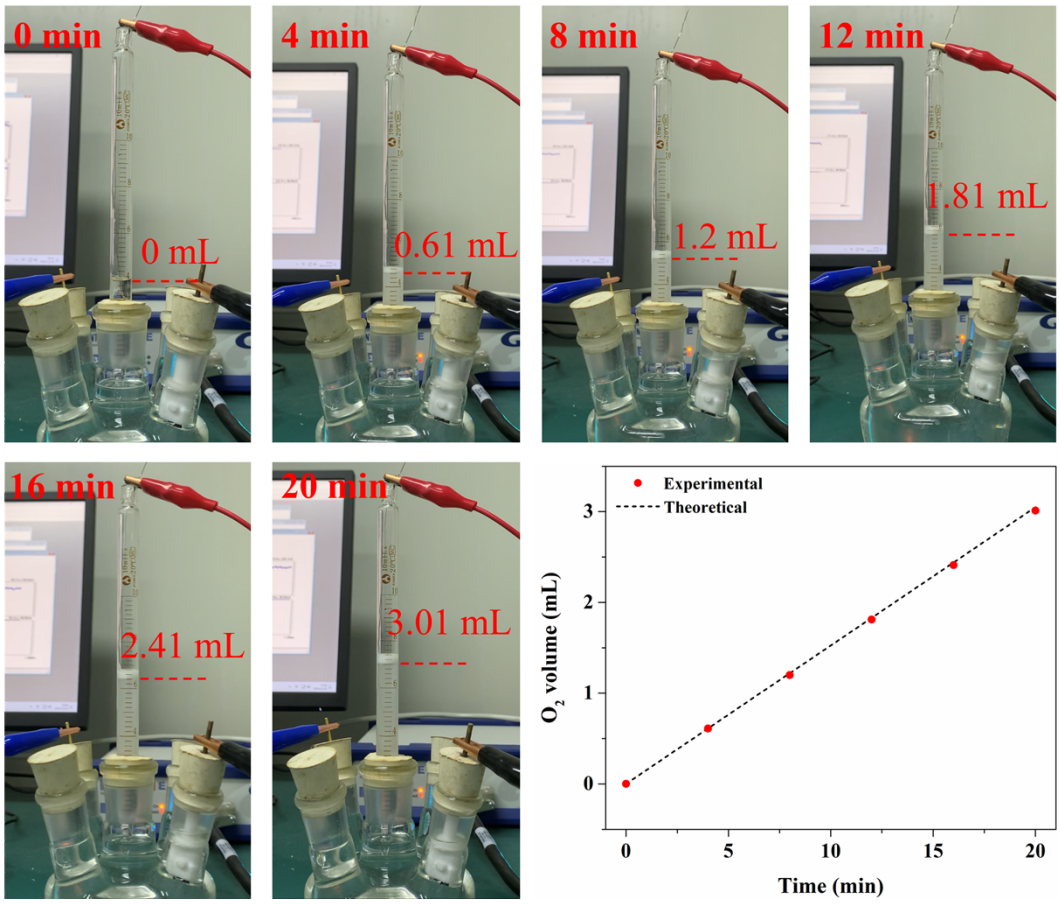

Supplementary Fig. 31. Measuring O_2 gas volume and determining the Faradaic efficiency by comparing experimental (red dot) and theoretical (black line) O_2 amounts using a drainage method during OER catalysis at 200 mA cm^{-2} in 1M KOH.

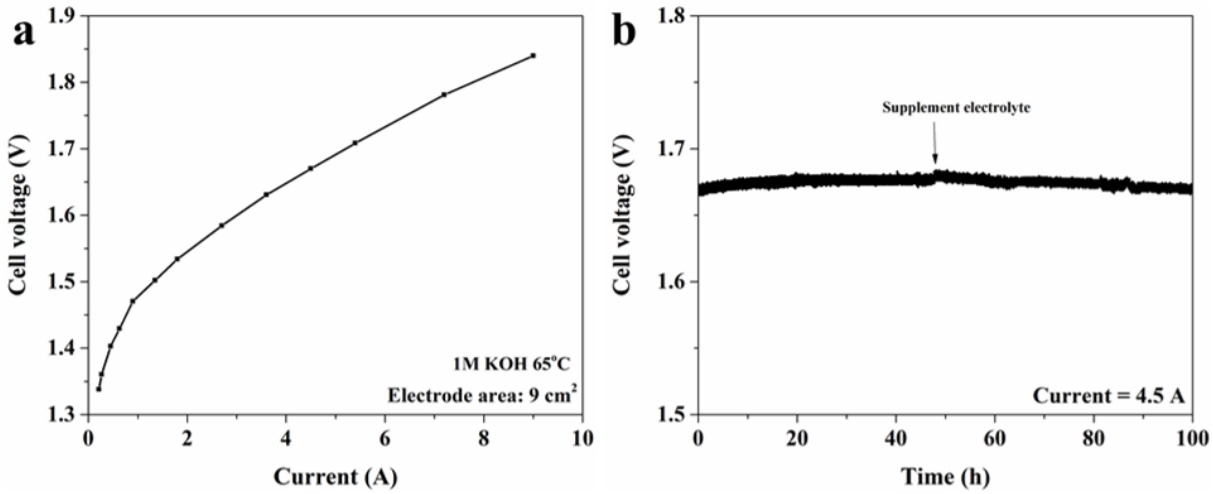

Supplementary Fig. 32. (a) The current vs. cell voltage for the anion-exchange-membrane water electrolyzer in 1 M KOH at 65 °C. (b) Long-term stability test under a constant current of 4.5 A in 1 M KOH at 65 °C.

Supplementary Table 1. The HER activity comparison between our work and other non-noble electrocatalysts in 1 M KOH. η_{100} and η_{500} mean the overpotentials at 100 and 500 mA cm^{-2}, respectively.

Electrocatalyst	η_{100} (mV)	η_{500} (mV)	Reference
$Fe/MoNi_4/MoO_2$	23	59	This work
$MoNi_4/MoO_2$	25	60	This work
$NiMoO_x/NiMoS$	89	174	*Nat. Commun.* **2020**, *11*, 5462
$Fe,P\text{-}NiSe_2$	83	141	*Adv. Mater.* **2021**, *33*, 2101425
FeNi-LDH/CoP	183*	265*	*Angew. Chem. Int. Ed.* **2019**, *58*, 11903
CoP-MNA	121	196*	*Adv. Funct. Mater.* **2015**, *25*, 7337
$Fe_{0.01}\text{-}Ni\&Ni_{0.2}Mo_{0.8}N$	59	135	*Energy Environ. Sci.* **2022**, *15*, 3945
Cu@NiFe LDH	192	-	*Energy Environ. Sci.* **2017**, *10*, 1820

Fe-CoP	162*	311*	*Adv. Mater.* **2017**, *29*, 1602441
Ni_3N@C	95*	222*	*J. Mater. Chem. A* **2021**, *9*, 13562
NiMoN@NiFeN	84	180	*Nat. Commun.* **2019**, *10*, 5106
Ni_3N/Co_3N/CoP	74	115	*Small* **2024**, *20*, 2311289
Co_3Mo/Cu	65*	111*	*Nat. Commun.* **2020**, *11*, 2940
NiMo/MoO_x	116*	254*	*Adv. Energy Mater.* **2019**, *9*, 1901454

"*" means the data was estimated from the literatures.

Supplementary Table 2. The fitted results of the EIS Nyquist plots for Fe/$MoNi_4$/MoO_2, $MoNi_4$/MoO_2, FeMo/MoO_2, MoO_2 and Ar-$NiMoO_4$ catalysts.

At -0.05 V	**Fe/$MoNi_4$/MoO_2**	**$MoNi_4$/MoO_2**	**FeMo/MoO_2**	**MoO_2**	**Ar-$NiMoO_4$**
R_s **(Ω)**	2.3	2.2	2.9	2.2	4.0
R_{ct} **(Ω)**	1.5	1.8	14.8	5.9	4.8
At 1.53 V	**Fe/$MoNi_4$/MoO_2**	**$MoNi_4$/MoO_2**	**MoO_2**		**Ar-$NiMoO_4$**
R_s **(Ω)**	2.3	2.4	2.5		2.5
R_{ct} **(Ω)**	0.2	0.4	11.5		20.7

Supplementary Table 3. Adsorption free energies of H and H_2O on $MoNi_4$, Fe/$MoNi_4$, Fe/MoO_2 and MoO_2 catalysts.

Models	$MoNi_4$	Fe/$MoNi_4$	MoO_2	Fe/MoO_2
ΔG_H (eV)	-0.70	-0.11	-1.03	-0.77
ΔG_{H_2O} (eV)	-1.66	-0.18	-0.93	-0.55

Supplementary Table 4. The OER activity comparison between our work and other non-noble electrocatalysts in 1 M KOH. η_{500} corresponds to the overpotentials at 500 mA cm^{-2} and

j_{300} means the current density at the overpotential of 300 mV.

Electrocatalyst	η_{500} (mV)	j_{300} (mA cm^{-2})	Reference
$Fe/MoNi_4/MoO_2$	277	1044	This work
$MoNi_4/MoO_2$	370	191	This work
$NiMoO_x$/NiMoS	278	682*	*Nat. Commun.* **2020**, *11*, 5462
Fe,P-$NiSe_2$	317	289*	*Adv. Mater.* **2021**, *33*, 2101425
Ni_2P-Fe_2P	322*	346*	*Adv. Funct. Mater.* **2021**, *31*, 2006484
$Ni_xFe_{1-x}Se_2$-DO	283*	615*	*Nat. Commun.* **2016**, *7*, 12324
NiMoN/NiFe LDH	236	1467*	*Nat. Commun.* **2023**, *14*,1873
Cu@NiFe LDH	312*	210*	*Energy Environ. Sci.* **2017**, *10*, 1820
NiMoN@NiFeN	337	207*	*Nat. Commun.* **2019**, *10*, 5106
Co_3Mo/Cu	414*	43*	*Nat. Commun.* **2020**, *11*, 2940
NiOOH@FeOOH	292	643*	*Adv. Mater.* **2022**, *34*, 2108619
NiOOH/(LDH/α-FeOOH)	366*	255*	*Adv. Mater.* **2023**, *35*, 2209338
NiFe-LDH/$NiFe_2O_4$	-	55*	*Angew. Chem. Int. Ed.* **2021**, *60*, 26829
FeNiOOH(Se)	350*	175*	*J. Am. Chem. Soc.* **2019**, *141*, 7005

" * " means the data was estimated from the literature.

Supplementary Table 5. The overall water splitting performance of different water electrolyzers made of non-noble electrocatalysts. The cell voltages at 100 and 500 mA cm^{-2} are denoted as V_{100} and $V_{500.}$

Electrocatalysts	V_{100} (V)	V_{500} (V)	Reference

$Fe/MoNi_4/MoO_2^{(+/-)}$	1.508	1.586	This work
$MoNi_4/MoO_2^{(+/-)}$	1.554	1.665	This work
$NiMoO_x/NiMoS^{(+/-)}$	1.62	1.75	*Nat. Commun.* **2020**, *11*, 5462
$Fe,P\text{-}NiSe_2^{(+/-)}$	1.599	1.733	*Adv. Mater.* **2021**, *33*, 2101425
$Ni_2P\text{-}Fe_2P^{(+/-)}$	1.682	1.865	*Adv. Funct. Mater.* **2021**, *31*, 2006484
NiMoN/NiFe LDH$^{(+/-)}$	1.538*	1.7	*Nat. Commun.* **2023**, *14*,1873
$EO\text{-}Co_3Mo^{(+)}\|\|Co_3Mo^{(-)}$	1.62	1.825*	*Nat. Commun.* **2020**, *11*, 2940
NiFe LDH@$Ni_3N^{(+/-)}$	1.63	1.8	*J. Mater. Chem. A* **2020**, *8*, 17202
$Fe_{0.01}\text{-}Ni\&Ni_{0.2}Mo_{0.8}N^{(+/-)}$	1.525	1.632	*Energy Environ. Sci.* **2022**, *15*, 3945
NiFe LDH-NS$^{(+/-)}$	1.8*	2.02*	*Adv. Mater.* **2017**, *29*, 1700017
$Co\text{-}Fe_2P^{(+/-)}$	1.69	1.8*	*Appl. Catal. B Environ.* **2021**, *297*, 120386
$MoS_2/FeCoNiP_x^{(+/-)}$	1.59	1.78*	*Nat. Commun.* **2021**, *12*, 1380
$Fe_2P/Co_2N^{(+/-)}$	1.561	1.663	*Adv. Funct. Mater.* **2023**, *33*, 2209465
NiFe LDH$^{(+)}$||NiO/Ni-CNT$^{(-)}$	1.584*	1.936*	*Nat. Commun.* **2014**, *5*, 4695

"*" means the data was estimated from the polarization curves given in the literature.

Reference

1. W. R. Zheng, *ACS Energy Lett.* **2023**, *8*, 1952.
2. Y. Yang, H. L. Fei, G. D. Ruan, J. M. Tour, *Adv. Mater.* **2015**, *27*, 3175-3180.
3. L. B. Wu, M. H. Ning, X. X. Xing, Y. Wang, F. H. Zhang, G. H. Gao, S. W. Song, D. Z. Wang, C. Q. Yuan, L. Yu, J. M. Bao, S. Chen, and Z. F. Ren, *Adv. Mater.* **2023**, *35*, 2306097.

4. G. Kresse, J. Hafner, *Phys. Rev. B* **1993**, *47*, 558.

5. J. P. Perdew, K. Burke, M. Ernzerhof, *Phys. Rev. Lett.* **1996**, *77*, 3865-3868.

6. S. Grimme, J. Antony, S. Ehrlich, H. Krieg, *J. Chem. Phys.* **2010**, *132*, 154104.

7. G. Henkelman, B. P. Uberuaga, H. Jónsson, *J. Chem. Phys.* **2000**, *113*, 9901-9904.